Boundary-Layer Meteorol (2007) 122:417–438
DOI 10.1007/s10546-006-9115-z

RESEARCH ARTICLE

Practical applicability of high frequency correction theories to CO_2 flux measured by a closed-path system

Takanori Shimizu

Received: 4 November 2005 / Accepted: 20 July 2006 /
Published online: 29 November 2006

Abstract The theoretical correction of CO_2 fluxes for high frequency attenuation in closed-path systems was re-summarized and its applicability examined using both measurements obtained at an Asiaflux forest site and empirical transfer functions used in previous studies. For our measurement system, the theoretical transfer function was applicable to high frequency correction, even when condensation occurred in the sampling line. Further, in respect to some measurement systems described in previous studies, it was found that the theoretical function was potentially applicable along with the empirical functions used. Meanwhile, in some systems significant errors could not be resolved by re-estimation of the theories. In these systems, because of undefined buffering effects, the actual response lag time decided by the maximum covariance method or by measurement of the system response time using tracer gas was significantly different from the lag time calculated from the tube dimensions and the measured flow rate. If the average flow rate calculated by the actual lag time was used to determine the theoretical function, the theoretical function became closer to, and sometimes agreed with, the empirical function. Any remaining deviation from each function might be associated with pressure fluctuations, but this problem was unable to be examined here. The results suggested that an empirical formulation for each site is considered applicable rather than a theoretical approach, although the theories are being developed to practical application.

Keywords Closed-path CO_2 flux · High frequency correction · Theoretical transfer function

1 Introduction

A method for high frequency correction is a major requirement in eddy covariance techniques, which have been routinely employed to estimate vertical fluxes of

T. Shimizu (✉)
Kyushu Research Center, Forestry and Forest Products Research Institute,
4-11-16 Kurokami, Kumamoto, Japan
e-mail: simizuta@affrc.go.jp

momentum, heat and mass in the atmospheric surface layer. The factors causing high frequency attenuation, such as sensor separation, scalar line-averaging, and a slow response sensor, were initially aggregated and described with simple equations by Moore (1986), with reference to earlier works (e.g. Kaimal et al. 1968; Kristensen and Jensen 1979). Although Moore's (1986) study contained some errors (Horst 1997, 2000), his approach has been recognized as a feasible solution. Massman (2000) improved the process to make it available for a closed-path eddy covariance system, which has been used for long-term measurements of scalar fluxes (e.g. Baldocchi et al. 2001). Massman incorporated the tube flow attenuation factor and the spectral phase shift factor, and approximated all the functions in a simple first-order form. In addition, Massman (2004) precisely described the characteristics of high frequency loss caused by an infrared gas analyzer (IRGA). The combination of these theoretical approaches, if applied to the correction of high frequency attenuation, enables a response to changes of wind speed, wind direction and flow rate in the sampling tube, which can occur either gradually or suddenly because of degradation, contamination and condensation in the sampling line and the measurement system. In spite of their advantage, most researchers who have used closed-path systems have applied an empirical frequency correction method to field measurements (e.g. Goulden et al. 1997; Hollinger et al. 1999), because of the prospect of buffering effects that are inexplicable with those theories. It is considered that these effects exist in the high frequency fluctuation of H_2O fluxes, which are significantly affected by tube degradations and/or contaminations (Leuning and Judd 1996). Consequently, for many study sites, the degradation of the high frequency signal of H_2O fluctuations becomes larger than that of CO_2 (e.g. Hollinger et al. 1999; Aubinet et al. 2001; Berger et al. 2001; Malhi et al. 2002; Su et al. 2004), although the high frequency attenuation for CO_2 can be expected to be slightly larger from tube flow theory (e.g. Massman 1991). Thus using an empirical function has been considered reasonable, and theoretical approaches have been treated, in a sense, as impractical propositions for the high frequency correction of trace gas fluxes measured by a closed-path system, not only for the H_2O flux but also for the CO_2 flux.

However, unlike H_2O fluctuations, it has been considered that tube degradation for high frequency attenuation of CO_2 fluctuations does not cause serious problems; a situation proven experimentally (Leuning and Judd 1996) and from the results of field measurements (Su et al. 2004). Further, for CO_2 fluxes, a theoretical correction was applied in some studies because the high frequency attenuation itself was not remarkable with their systems (Berger et al. 2001; Cook et al. 2004), while there were other studies that reported definite gaps between theoretical approaches and the ratio of the (co)spectrum obtained from their field observations (Aubinet et al. 2001; Yasuda and Watanabe 2001). Thus, more careful examinations are needed to determine the applicability of these theories to high frequency corrections for closed-path CO_2 fluxes. The present paper initially reviews and summarizes theoretical transfer functions including the newly developed theories of Massman (2004). Then, in order to check the applicability of the theories to a measurement system, theoretical correction is examined using datasets obtained at an Asiaflux forest site. Tests are also performed on data acquired when the flow rate was reduced by condensation within the sampling line. Discussion is carried out concerning the applicability and limitations of a theoretical approach to high frequency correction of closed-path CO_2 fluxes by comparing some empirical transfer functions applied in previous studies.

2 Theories

2.1 Correction functions for individual factors

The transfer function for high frequency correction (TF) can be represented by a combination of individual transfer functions for certain factors associated with high frequency attenuation (Moncrieff et al. 1997). TF is generally expressed in the form

$$\mathrm{TF}(\omega) = h_{\mathrm{lat}}(\omega)h_{\mathrm{lon}}(\omega)h_{\mathrm{line}}(\omega)h_{\mathrm{tube}}(\omega)h_{\mathrm{3B}}(\omega)h_{\mathrm{vol}}(\omega)\mathrm{e}^{-\mathrm{j}\phi(\omega)}, \tag{1}$$

where $\omega = 2\pi f, f$ is the natural frequency, $h(\omega)$ are individual transfer functions for certain factors, and the subscripts represent factors as described below. The functions commonly related with eddy covariance systems, i.e., lateral and longitudinal sensor separations and sensor line-averaging, were first summarized by Moore (1986), and then partly corrected by Horst (1997). The functions for the lateral and longitudinal separation of two sensors, $h_{\mathrm{lat}}(\omega)$ and $h_{\mathrm{lon}}(\omega)$ are given by

$$h_{\mathrm{lat,\,lon}}(\omega) = \exp\left\{-9.9\left(\frac{\omega\, l_{\mathrm{lat,\,lon}}}{2\pi u}\right)^{1.5}\right\} \tag{2}$$

where $l_{\mathrm{lat,\,lon}}$ is the lateral and longitudinal distance of the sensors, and u is the wind speed. Here the form of $h_{\mathrm{lon}}(\omega)$ is supposed to be the same as that of $h_{\mathrm{lat}}(\omega)$, with the assumption that $h_{\mathrm{lat}}(\omega) = h_{\mathrm{lon}}(\omega)$ is useful for small sensor separation (Moore 1986).

The functions for sensor line-averaging effects are

$$h_{\mathrm{line(s)}}(\omega) = \frac{1}{(\omega p/u)}\left[3 + \exp(-\omega p/u) - \frac{4\{1 - \exp(-\omega p/u)\}}{(\omega p/u)}\right] \tag{3}$$

for a scalar quantity, where p is the sensor path length, and

$$h_{\mathrm{line(v)}}(\omega) = \frac{4}{(\omega p/u)}\left[1 + \frac{\exp(-\omega p/u)}{2} - \frac{3\{1 - \exp(-\omega p/u)\}}{2(\omega p/u)}\right], \tag{4}$$

is the vector quantity. Note that $h_{\mathrm{line(s)}}(\omega)$ in Eq. 3 is the function for $\theta = 90°$, where θ is the angle between the sensor path and the wind vector, and $h_{\mathrm{line(v)}}(\omega)$ in Eq. 4 is the function for the vertical wind vector. For closed-path scalar fluxes, $h_{\mathrm{line(s)}}(\omega)$ is negligible.

In addition to these factors, tube flow attenuation needs to be estimated for closed-path flux measurements. The tube flow correction function $h_{\mathrm{tube}}(\omega)$ can be represented by the following general form:

$$h_{\mathrm{tube}}(\omega) = \exp(-\omega^2 r\Lambda L_{\mathrm{t}}/U_{\mathrm{t}}^2) \tag{5}$$

where r is the inner tube radius, Λ is an attenuation coefficient, L_{t} is the tube length and U_{t} is the tube flow velocity. Consider pipe flow: turbulent flow occurs when the Reynolds number (Re) is above 2300, where $Re = 2rU_{\mathrm{t}}/\upsilon$ and υ is kinematic viscosity. According to Aubinet et al. (2000) (quoting from Lenschow and Raupach 1991; and Leuning and King 1992), the attenuation coefficient Λ for laminar tube flow, i.e. the flow with $Re < 2300$, is expressed as

$$\Lambda = rU_{\mathrm{t}}/48D_{\mathrm{s}} \tag{6}$$

where D_{s} is the molecular diffusivity of the tracer gas (here CO_2). Note that D_{s} for H_2O is larger than CO_2 and consequently the attenuation of H_2O fluctuations

should be small under ideal conditions for laminar flow. The Λ for turbulent tube flow ($Re \geq 2300$) is

$$\Lambda = 20Re^{-1/8}/\pi^2, \tag{7}$$

where the differences between H_2O and CO_2 are not reflected. In the case of turbulent tube flow, Massman (1991) proposed an alternative theory in which a continuous approach was postulated from laminar to turbulent flow through the transition region ($Re \cong 2300$). Leuning and Judd (1996) used the results from Massman (1991) to formulate the frequency at which the tube flow function is $2^{-1/2}$. From their formulation for CO_2, Λ can be approximated as follows:

$$\Lambda = \frac{0.693}{8\pi^2\left[\ln(0.75Re^{0.04})\right]^2}. \tag{8}$$

A similar function for H_2O was also obtained by Leuning and Judd (1996), with the coefficients 0.75 and 0.04 in Eq. 8 replaced with 0.76 and 0.039; this also leads to a slightly smaller Λ for H_2O than for CO_2 when Re is not extremely large. The Λ represented by Eq. 8 allows for a continuous approach from laminar flow to turbulence, and is applied for turbulent tube flow for the following sections, rather than Eq. 7.

The high frequency attenuation caused by an IRGA, including the signal processing and the volume averaging effects of the IRGA chamber, was described in detail and summarized by Massman (2004). Noting that the most widely used IRGA, the LI-6262 (LI-COR, USA), uses a third-order Bessel filter as an anti-aliasing filter for signal output, the transfer function, $h_{3B}(\omega)$, is expressed as

$$h_{3B}(\omega) = 15/\{(15 - 6\Omega^2) - \mathbf{j}(15\Omega - \Omega^3)\} \tag{9}$$

where $\mathbf{j}$ is the imaginary unit, $\Omega = 3.0824\tau_{3B}(\omega/2\pi)$ and τ_{3B} is the time constant of the third-order Bessel filter. Following Massman (2004), $\tau_{3B} = 0.2$ s is used in this study. The spectral transfer function related to volume averaging for an IRGA chamber is

$$h_{vol}(\omega) = \frac{\sin^2(\omega\,\tau_{vol}/2)}{(\omega\,\tau_{vol}/2)^2}, \tag{10}$$

where τ_{vol} is the time constant of the volume averaging effect. In the following analysis, the minimum value of $\tau_{vol} = V_{cham}/\pi r^2 U_t$ is used, where V_{cham} is the volume of an IRGA chamber (for LI-6262, 1.19×10^{-5} m^3). It should be noted that the phase shift caused by τ_{vol} is not explicitly expressed in Eq. 10.

The phase shift caused by the tube intake and the sensor separation in the wind direction are commonly expressed as an exponential complex function of $\exp\{\mathbf{j}\phi(\omega)\}$ (Massman 2000). Here $\phi(\omega)$ is

$$\phi(\omega) = \omega(L_t/U_t + l_{lon}/u), \tag{11}$$

where l_{lon} is the longitudinal separation of the sensors. Note that L_t/U_t is usually removed by the digital shifting of a sonic anemo-thermometer time series.

The transfer functions for those factors described above were summarized in the same form, a function for a first-order filter, by Massman (2000). The form is given by

$$h_{t_1}(\omega) = 1/(1 - \mathbf{j}\omega t_1), \tag{12}$$

where t_1 is the equivalent time constant of a factor associated with high frequency attenuation. If the phase shift is negligible, Eq. 12 can be represented as

$$h_{t_1}(\omega) = 1/(1 + \omega^2 t_1^2). \tag{13}$$

The filter time constants for the first-order type function equivalent to $h_{\mathrm{lat}}(\omega)$, $h_{\mathrm{lon}}(\omega), h_{\mathrm{line(s)}}(\omega), h_{\mathrm{line(v)}}(\omega)$ and $h_{\mathrm{tube}}(\omega)$ for the turbulent tube flow were given by Massman (2000), here identified as $t_{\mathrm{lat}}, t_{\mathrm{lon}}, t_{\mathrm{line(s)}}, t_{\mathrm{line(v)}}$ and t_{tube}, respectively. Additionally, the time constants for IRGA signal processing (t_{IRGA}), for the volume averaging effect of an IRGA chamber ($t_{1\mathrm{vol}}$), and t_{tube} for the laminar tube flow are examined and determined in Appendix A. When the first-order function is chosen for high frequency correction, TF(ω) can be written as below (Massman 2000), taking into account that the squares of the time constants can be neglected. The function is then be given by

$$\mathrm{TF}(\omega) = \left[1/(1 + \omega^2 t_{\mathrm{e}}^2)\right] \mathrm{e}^{-\mathbf{j}\phi(\omega)} \tag{14}$$

where $t_{\mathrm{e}} = (t_{\mathrm{tube}}^2 + t_{\mathrm{lon}}^2 + t_{\mathrm{lat}}^2 + t_{\mathrm{line(v)}}^2 + t_{\mathrm{IRGA}}^2 + t_{1\mathrm{vol}}^2)^{1/2}$ involves the root of the sum of the squares of the equivalent time constants of the factors.

In addition to the factors related to high frequency correction, which are described above, several other factors associated with the WPL correction (Webb et al. 1980) were recently proposed, such as the effect of overcorrection of the water vapour covariance term, and that of ignoring pressure fluctuations within an IRGA chamber (Massman 2004). These effects become considerable if the tube flow is turbulent and/or if some conditions (temperature, humidity and/or air pressure) in the sample air are directly affected by ambient conditions. However, because it is difficult to apply them to the results of previous studies, these factors are disregarded in the present study.

3 Site and data

The observation site, the Kahoku Experimental Watershed (KHEW), is part of the Asiaflux network, a planted coniferous forest located on Kyushu Island in south-west Japan (33°08′N, 130°43′E). The island is characterized by very high precipitation for the warm temperate regions, with mean air temperature and annual precipitation from 2000 to 2003 of 15.2°C and 2080 mm year^{-1}, respectively. CO_2 flux measurements were conducted using a 50 m-tall meteorological tower, which stands within WS2 in Fig. 1, adjacent to WS3, the research site of Shimizu et al. (2003). The distribution pattern of plant species around the tower site is the same as WS3, i.e., Japanese cypress (*Chamaecyparis obtusa*) stands on the ridge area and Japanese cedar (*Cryptomeria Japonica*) from the valley to the hillside. However, the growth of the trees in WS2 is rather better than that in WS3, and the tree height is about 32 m beneath the tower. A sonic anemo-thermometer (DAT-600, KAIJO, Japan) and a gas intake mouth were installed at the top of the tower, and the separation between the vertical axis of the sonic and the mouth was 0.55 m until December 2003.

Figure 2 schematically represents the design of the KHEW air sampling system, whose construction was based on Yasuda and Watanabe (2001). The sample air was drawn from the mouth through a 57 m long and 6 mm inner diameter Teflon® tube at the normal flow rate of 7–8 l min^{-1}. After an exhaust port, the flow rate was

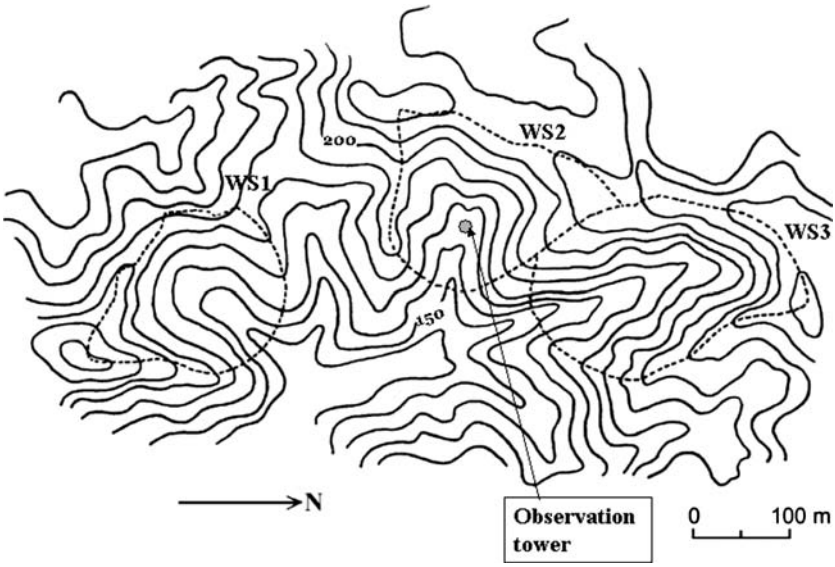

Fig. 1 Topographical map of the Kahoku experimental watershed (KHEW)

controlled to 2 l min^{-1} through a 3.5 m long and 4 mm inner diameter Teflon® tube. In the pathway of the 4 mm tube, the sample was dried by two serially connected driers (MD-110-48F, Perma Pure Inc., USA), whose total length and inner diameter were 2 m and 2 mm, respectively, and finally carried to the IRGA (LI-6262) chamber. Analogue outputs of the sonic and the IRGA were recorded at 10 Hz using a data logger (DR-M3b, TEAC, JAPAN).

Turbulence variables of vertical wind (w', where the dash denotes the fluctuating variable), virtual temperature (T') and closed-path CO_2 concentration (C') were calculated from the residuals of a 30-min block average, after correction of the sonic transducer shadow (Shimizu et al. 1999). As shown in Fig. 1, the site was located on rolling terrain, and planar fit coordination was performed for the calculation of w'. The coordinate process was the same as described in Aubinet et al. (2005), but using a polynomial as a fitting function instead of a sinusoidal function. The phase shift factors, represented in Eq. 11 and included in the third-order Bessel filter, are corrected before analysis, determining the tube flow delay by a trial-and-error test to maximize the w'–C' correlation.

For the following analysis, two of the 1-month datasets were used; the dataset of Period 1 was obtained from July 4 to August 11 in 2000, and that of Period 2 from April 2 to May 6 in 2003. Within Period 2, the tube flow rate was seriously reduced but the fluctuation of the flow rate was expected to be relatively small, according to the lag time test carried out on data obtained at 1200–1230 local time each day.

A given 30-min data average was screened by the following criteria before it was accepted for further analysis; the first criterion required that friction velocity u_* was higher than 0.35 m s^{-1} when observations were acquired; the next criterion required that absolute values of sensible heat and CO_2 fluxes, which were tentatively calculated without any correction procedure, were more than 50 W m^{-2} and 0.18 mg CO_2 m^{-2} s^{-1}, respectively. Further, if the cospectral peak emerged in a

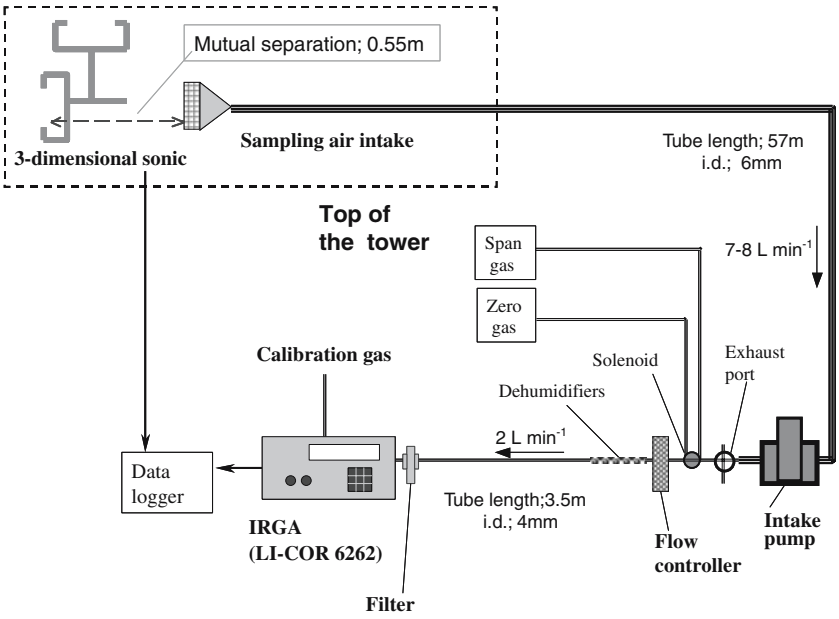

Fig. 2 Schematic image of the Kahoku experimental watershed (KHEW) sampling system

frequency range lower than 0.0005 Hz or higher than 0.25 Hz, the data were eliminated from the analysis. The number of spikes for all variables (w', T' and C') was also applied as a criterion and was set to less than 180 (equal to 1%). The spikes were regulated by the method of Schmid et al. (2003), but the minimum width of the local data window, which was applied to determine consecutive flagged values as spikes, was decided at 20 s.

4 Results and discussion

4.1 Applicability of the theory to the sample data

From the data screening, the numbers of usable 30-min data were 123 for Period 1, and 148 for Period 2. The average and the standard deviation of the flow rate calculated from the usable data were $7.8 \pm 0.02\,\mathrm{l\,min^{-1}}$ (Period 1) and $2.12 \pm 0.018\,\mathrm{l\,min^{-1}}$ (Period 2). The flow rate in Period 2 apparently decreased, possibly due to condensation that was found in the connection of the tube near the exhaust port after the period finished. Figure 3 shows the values of the ensemble averages of frequency weighted cospectra of wT and that of wC for each measurement period, normalized by the sum of the cospectrum within a range of 0.0025–0.0125 Hz. In Fig. 3, the sonic line-averaging effects were corrected only for the wT cospectrum. Note that here Eqs. 3 and 4 were applied as approximate expressions, although the direction of the w wind component was not strictly consistent with the sonic vertical axis because of coordinate rotation. The figures suggest that cospectral similarity between virtual temperature and CO_2 fluxes can be assumed at the lower frequency range for both periods. Then

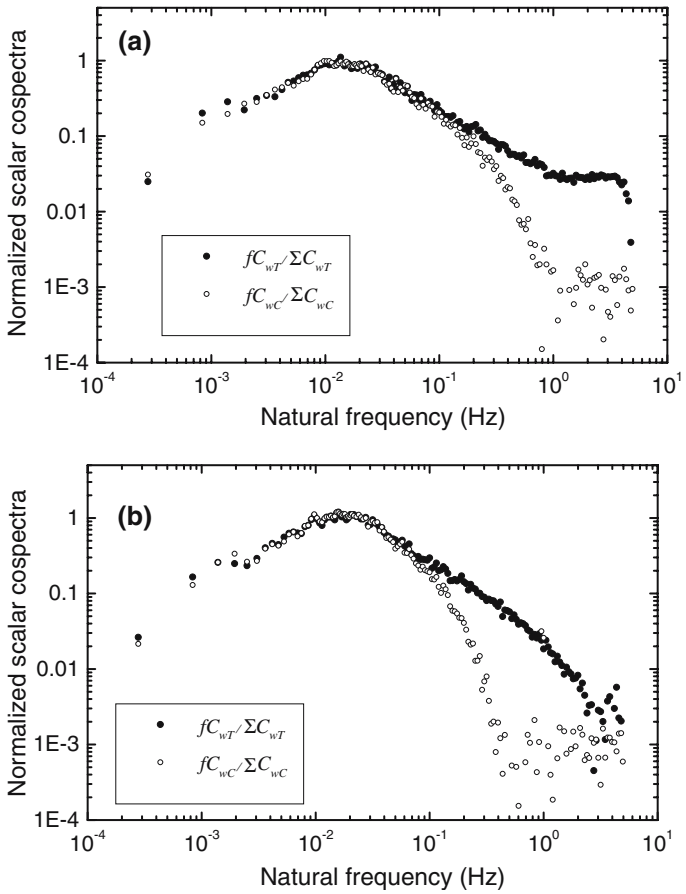

Fig. 3 Ensemble averages of normalized scalar cospectra of sensible heat (black circle) and CO_2 (open circle) from usable data measured at the Kahoku experimental watershed (KHEW) site; (**a**) flow rate 7.81 min^{-1} (within nominal state), (**b**) flow rate 2.11 min^{-1} (reduced by condensation), respectively

the ratio of the normalized cospectum of wT to that of wC is used for the following comparison. The damping of CO_2 fluctuations in Period 2 was remarkably larger than that in Period 1 at the higher frequency range.

The theoretical function, the ratio of normalized cospectra and the empirical function fitted to the ratio of cospectra are plotted together in Fig. 4. The theoretical function used here is the multiplication form of Eq. 1. The theoretical function was actually determined for each of the 30-min data periods, but the representative curves are drawn in Fig. 4 on the basis of the averages of wind speed, wind direction and flow rate. The empirical transfer function $TF_e(\omega)$ was set to the exponential form, as $TF_e(\omega) = \exp(A\omega/2\pi)^B$, where A and B are fitting parameters. The average corrections for the CO_2 fluxes were 3.9% and 4.7% for Periods 1 and 2, respectively, when using the theoretical function; if the exponential functions are applied, the correction factors are 4.2% and 5.6% for Periods 1 and 2, respectively. The theoretical function slightly underestimated the correction factor compared to the empirical function, and

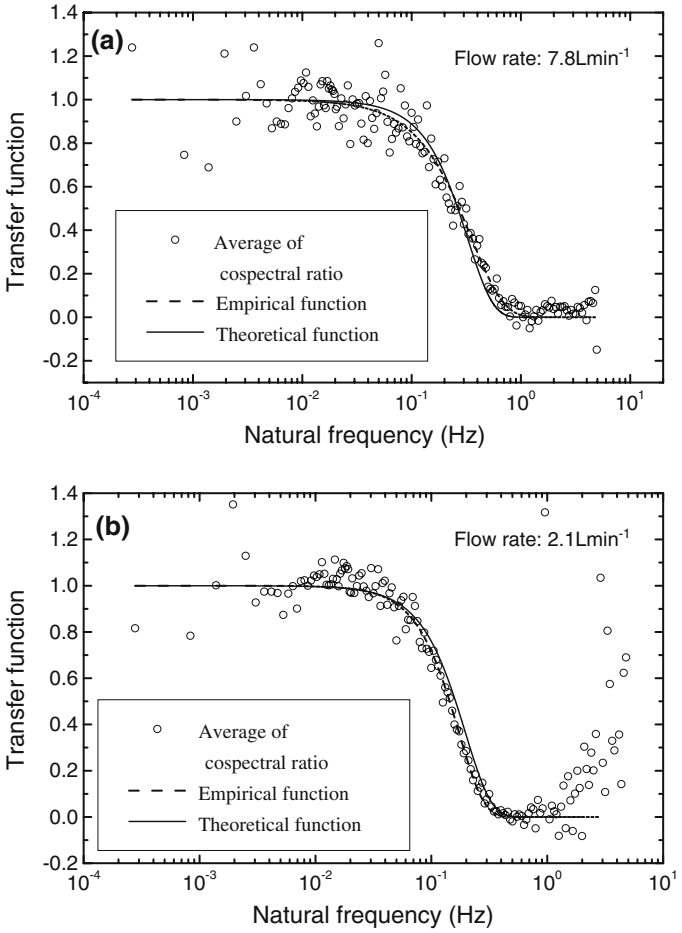

Fig. 4 High frequency correction functions and the ratio of the normalized cospectra averaged from all usable data (open circles). Black line: theoretical function and dashed line: exponential function fitted to the circles. The distributions of the upper (**a**) and lower (**b**) panels are the same as in Fig. 3

the trend was clearer in Period 2, when condensation occurred within the sample line. The slight deviation might be caused by some minor factors that are still not considered in the theories. These factors, although not so affected in the KHEW measurement system, might be significant in some systems introduced in the following section. Further, the uncertainty of the theoretical function must be more or less increased by condensation, as was the case at the KHEW site. However, in the case of our measurement at KHEW, the error was relatively small and within an allowable range, since the same extent of uncertainty might have been caused by other procedures for flux computation. Thus, it can be concluded that the theoretical function could be applied to the high frequency correction of the closed-path CO_2 flux, at least to that measured at the KHEW site, even when the flow rate was decreased by condensation.

Considering that the data in Period 2 were obtained under such severe conditions where the flow rate of the sample line was reduced to almost the same rate as the

flow-controlled line, the result suggests that the quality of CO_2 concentration data may not be degraded by condensation within a sample line. This characteristic might be general for CO_2 data measured in any system, and, if so, although CO_2 flux data obtained under rainy conditions have been excluded by some researchers (e.g., Hollinger et al. 1999), it should not necessarily be excluded from further analysis if the data have been screened by some form of quality control. However, this tendency might be peculiar to CO_2 data. The damping of high frequency fluctuations caused by condensation would obviously be fatal for the water vapour flux, and this should be verified before high frequency corrections are applied to other tracer gases, such as methane or ozone.

4.2 Comparisons with previous studies

In this section several measurement systems and sites described in previous studies, which are listed in Table 1, are applied to extend discussions of applicability and limitation of the theoretical approach for high frequency correction of closed-path CO_2 fluxes. The characteristics of the KHEW in this study are also in the same table. Except for some minor specifications, all of these studies gave detailed descriptions of their measurement systems and of the empirical transfer functions that were used. Generally, an empirical transfer function for a high frequency correction is a complex form, as is the theoretical function. It can be represented by two components, a gain function $g(\omega)$ and a phase function $p(\omega)$ (e.g. Watanabe et al. 2000), viz.

$$\mathrm{TF}(\omega) = g(\omega)\exp\{\mathbf{j}p(\omega)\}. \tag{15}$$

Details of the empirical functions applied in the previous studies are given in Appendix B.

4.2.1 Impact of atmospheric conditions on flux errors

Initially, ideal and moderate conditions are assumed in the comparisons between theoretical and empirical functions from previous studies, except for the Chequamegon-Nicolet National Forest (ChNNF) system in which the high frequency attenuation for CO_2 flux was not so remarkable and was masked by the instrumental noise with a theoretical function applied for high frequency correction (Cook et al. 2004). In Fig. 5, the theoretical functions represented in Eq. 1 are drawn on the basis of the specifications in Table 1, and on the assumption that the atmospheric surface layer is neutral, air temperature is set at 20°C, atmospheric pressure is 1 atm at sea level, with a rate of decrease with height of $0.12\,\mathrm{hpa\,m^{-1}}$, and the wind direction is 45° toward the array of sensors (equivalent to $l_{\mathrm{lon}}/u = l_{\mathrm{lat}}/u$) and $u_* = 0.35\,\mathrm{m\,s^{-1}}$. The wind speed is determined from the logarithmic wind law, with the assumed values of zero plane displacement $d = 0.75h$ and roughness length $z_0 = 0.08h$, where h is vegetation height. The empirical function for BOREAS-NSA-OBS (hereafter NSA-OBS, Goulden et al. 1997) crosses the theoretical function (Fig. 5a). As for the 46m-height of the UMBS (hereafter UMBS-46m, Su et al. 2004), the functions accord with each other in the relatively lower frequency region, while the deviation becomes larger in the higher frequency region (Fig. 5d). Meanwhile, as shown in Fig. 5b and c, for the system of Kawagoe (Yasuda and Watanabe 2001) and for that of Vielsalm (Aubinet et al. 2001), the theoretical functions remarkably underestimate the correction factor over the whole frequency range where attenuation occurs.

Table 1 General information of closed-path flux measurement systems for several observation sites

Site	Vegetation	Elevation (m)	Height of canopy (m)	Measurement height (m)	Sub-sample system	Tube length (main sample/ subsample line) (m)	Inner tube diameter (main sample/ subsample line) (mm)	Flow rate (before/after subsample drawn) ($l\,min^{-1}$)	Distance between sensors (m)	Reference
BOREAS-NSA-OBS <NSA-OBS> (Canada)	Boreal black spruce forest	259	10	29	Applied	50 / 1.7[a]	6.4/4	16–18/4	0.5	Goulden et al. (1997)
Kawagoe (Japan)	Temperate deciduous forest	30	15	20	Applied	28 / 3.1+ 1.895[b]	6/4	14/2	0.15	Yasuda and Watanabe (2001), http://wwwcger2.nies.go.jp/asiaflux
Vielsalm (Belgium)	Mixed forest (Dougras fir and Beech)	450	27–35	40	None	8	4	8	Not described[c]	Aubinet et al. (2000), Aubinet et al. (2001)
UMBS 46 m height (USA)	Mixed hardwood and boreal forest	234	22	46	None	52	4.8	6–7	Not described[c]	Schmid et al. (2003), Su et al. (2004)
Chequamegon-Nicolet National Forest <ChNNF> (USA)	Upland hard wood forest	515	24	30	None	4	3.96	3	Not described	Berger et al. (2001), Cook et al. (2004)
Kahoku Experimental Watershed <KHEW> (Japan)	Coniferous forest (Cedar and Cypress)	165	32	51	Applied	57/ 3.5 + 2[b]	6/4	7–8/2	0.55	This study

[a] Values recalculated by applying the flow rate, the standard delay time and the inner tube diameters published in the corresponding literature
[b] Dehumidifier tube with 2 mm i.d. (Kawagoe: connected parallel, KHEW: connected serially)
[c] 0.15 m is assumed for the theoretical function calculation

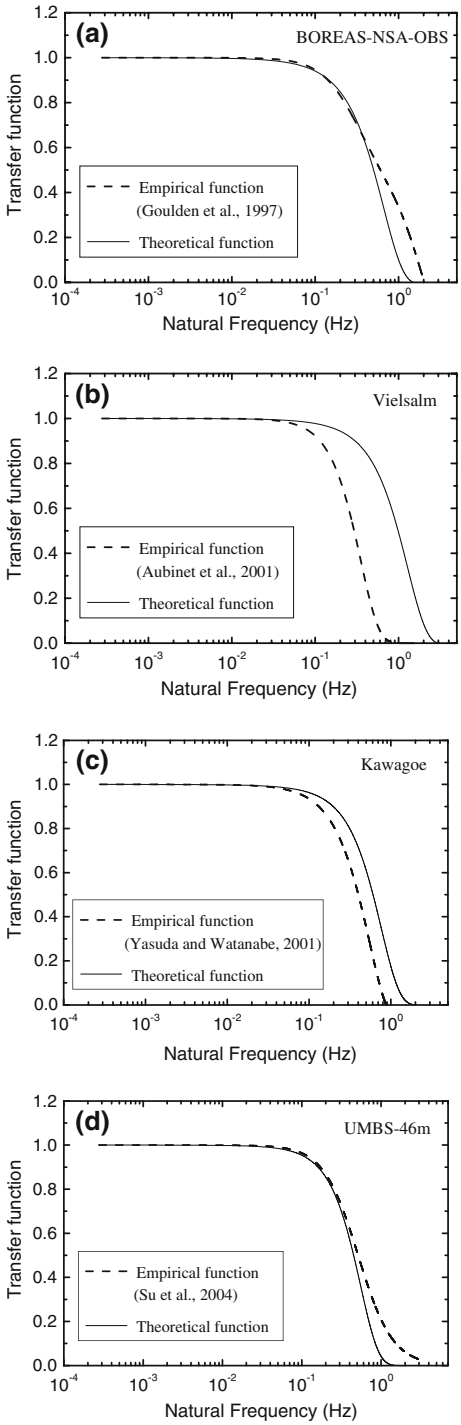

Fig. 5 Comparison of the theoretical function (black line) with the empirical function (dashed line) applied in earlier studies under conditions assumed in the text; (**a**) R-C filter function represented for BOREAS-NSA (Goulden et al. 1997), (**b**) exponential function for Vielsalm (Aubinet et al. 2001), (**c**) exponential function for Kawagoe (Yasuda and Watanabe 2001), and (**d**) a first-order type function for UMBS-46m (Su et al. 2004)

The percentage of the correction factors would be most affected by wind speed and atmospheric conditions rather than other environmental conditions, because these are closely related to the shape of the scalar cospectrum. If wind speed increases, or if the atmospheric conditions become stable, the peak of the cospectrum shifts to the high frequency region, and the difference of the transfer functions on the flux values will have a significant impact. The effect of these conditions on the correction factors has been quantified theoretically and experimentally in previous works (e.g. Lee and Black 1994; Kristensen et al. 1997; Goulden et al. 1997). For NSA-OBS, the high frequency correction caused a 15–30% difference in the flux estimation under stable conditions, while it was 2–10% during daytime. Thus, the percentage of the flux differences caused by using the theoretical functions would be larger under higher wind speed and/or more stable atmospheric conditions. To estimate the trend for each site, four types of atmospheric conditions are assumed: the neutral conditions described above, slightly unstable conditions with $(z-d)/L = -0.2$ and $u_* = 0.7\,\mathrm{m\,s^{-1}}$, slightly stable conditions with $(z-d)/L = 0.1$ and $u_* = 0.3\,\mathrm{m\,s^{-1}}$, and moderately stable conditions with $(z-d)/L = 0.75$ and $u_* = 0.15\,\mathrm{m\,s^{-1}}$, where z is the observation height and L is the Obukhov length. The effect of wind speed on the cospectral shift is estimated from a comparison of the first two conditions, and the effect of atmospheric stability can be shown by a comparison of all the conditions except for the unstable one. The wind speed u is determined as

$$u = \frac{u_*}{\kappa}\left(\ln\frac{z-d}{z_0} - \Psi_\mathrm{m}\right) \tag{16}$$

where κ is von Karman's constant ($= 0.4$), Ψ_m is the integral Monin–Obukhov stability correction function for momentum, used here as

$$\Psi_\mathrm{m} = \ln\left(\frac{0.28 + y^{0.75}}{0.28 + (0.0059 + y_0)^{0.75}}\right) - 1.29[y^{1/3} - (0.0059 + y_0)^{1/3}] \tag{17}$$

for unstable conditions (Brutsaert 1992) where y and y_0 are $-(z-d)/L$ and $-z_0/L$, respectively, and

$$\Psi_\mathrm{m} = -5\left(\frac{z-d}{L} - \frac{z_0}{L}\right) \tag{18}$$

for stable conditions (Dyer 1974). Cospectral density function should also be assumed to estimate the difference of flux values, and the forms of the functions applied here are

$$\frac{fC_{wx}(f)}{\overline{w'x'}} = \frac{\beta_{-1} f(z-d)/u}{[1 + \beta_{-2} f(z-d)/u]^2}, \tag{19}$$

for neutral and unstable conditions, where $C_{wx}(f)$ is the scalar cospectrum, x is a certain scalar (here CO_2) and β_{-1} and β_{-2} are fitting parameters, and

$$\frac{fC_{wx}(f)}{\overline{w'x'}} = \frac{\beta_{+1} f(z-d)/f_0 u}{[1 + \beta_{+2} f(z-d)/f_0 U]^{2.1}}, \tag{20}$$

where

$$f_0 = \left[a_{+1}\left(1 + 6.4\frac{z-d}{L}\right)\right]^{3/4}, \tag{21}$$

for stable conditions, and β_{+1}, β_{+2} and a_{+1} are fitting parameters (Su et al. 2004). The parameters vary with $z - d$ and vegetation conditions (Sakai et al. 2001: Su et al. 2004), and for UMBS-46 m, $\beta_{-1} = 8.2$ and $\beta_{-2} = 8.9$ $\beta_{+1} = 1.58$, $\beta_{+2} = 1.41$ and $a_{+1} = 0.151$ (Su et al. 2004); these values are applied here for NSA-OBS due to the similar value of $z - d$ for UMBS-46 m. For Kawagoe and Vielsalm, β_{-1}, β_{-2}, β_{+1}, β_{+2} and a_{+1} are set as 10.4, 10.6, 2.04, 1.71 and 0.113, respectively, with reference to the results obtained from measurements at another height (32 m) at the UMBS site (Su et al. 2004).

Table 2 shows the calculated wind speed and the trend of flux errors caused by using the theoretical functions under assumed conditions. Here the high frequency correction is limited from the region of $f < 0.01$ Hz to the point where each transfer function is 0.05. Because the empirical functions were determined from field measurements, the error trend might depend on the deviation of the assumed conditions from realistic patterns at each site. But, in common, the largest error emerged under rather stable atmospheric conditions. However, under strongly stable conditions, the CO_2 flux itself becomes much less significant due to lack of turbulence and the relative increase of storage terms and of vertical and horizontal advection (e.g. Lee 1998; Finnigan 1999; Aubinet et al. 2005). It is to be reasonably expected that data obtained under strongly stable conditions will be eliminated when the empirical functions are determined. In this sense, for the systems in which the expected errors were within 1.5% under unstable and neutral conditions, namely for NSA-OBS and UMBS-46 m, theoretical functions as well as empirical ones might be applicable. Meanwhile, for Kawagoe and Vielsalm, the underestimation errors become 2–4% under neutral and unstable conditions. The volume averaging effect of the IRGA chamber was not enough to compensate for the gap between theoretical predictions and the empirical functions as presumed in both studies. These results suggest that theoretical high frequency correction might be acceptable for some measurement systems, while there are some systems in which significant differences would remain in flux calculations between theoretical and empirical functions.

4.2.2 Buffering effect in the sampling line

The Kawagoe sampling system was almost the same as that at the KHEW site, while the system used at Vielsalm was similar to that at the ChNNF, with no flow control, relatively short tube length and only membrane filters from the intake mouth to the

Table 2 Errors caused by using the theoretical transfer function instead of the empirical function for each site. Plus and minus signs represent overestimation and underestimation of the correction factor, respectively

Sites	Assumed conditions			
	$z/L = -0.2$, $u_* = 0.7\,\mathrm{m\,s^{-1}}$	$z/L = 0$, $u_* = 0.35\,\mathrm{m\,s^{-1}}$	$z/L = 0.2$, $u_* = 0.3\,\mathrm{m\,s^{-1}}$	$z/L = 0.75$, $u_* = 0.1\,\mathrm{m\,s^{-1}}$
NSA-OBS	+0.4%	+1.4%	+2.0%	+3.4%
Kawagoe	−4.6%	−2.6%	−4.6%	−8.7%
Vielsalm	−3.5%	−2.2%	−4.1%	−8.2%
UMBS-46 m	+1.0%	+0.7%	+1.3%	+2.3%

Table 3 Flow speed, Reynolds numbers and lag times for the measurement systems listed in Table 1

Site	Flow velocity in main sample tube ($m\,s^{-1}$)	Reynols number in main sample flow (20°C, 1 atm a.s.l.)	Expected lag time calculated by tube length, diameter and flow rate (s)	Actual response lag time, typical (s)
BOREAS-NSA	8.3–9.3	3606*	5.7–6.3	6
Kawagoe	8.3	3260	4.5	7.4
Vielsalm	10.6	2648	0.75	2.5
UMBS-46 m	5.5–6.4	1840*	8.0–9.4	8
ChNNF	4.1	997	0.7	1.3
KHEW	4.1–4.7	1870*	13.6–15.3	13.8

*The median value of flow velocity is used for the calculation.

IRGA. Nevertheless, a theoretical high frequency correction could be applied to the KHEW and ChNNF sites. For further comparisons, Table 3 lists the values of flow velocity and *Re* calculated from the specifications in Table 1, with information about lag times. In Table 3, 'actual response lag time' means the representative delay time described in each report, which in each system would be decided either by digital time shifting until the occurrence of the maximum w'–C' covariance or by the measured response time of the IRGA from the input of tracer gas at the intake mouth. While 'expected lag time' is calculated from the nominal flow rate, the tube length and inner diameter are listed in Table 1. The common characteristics of the systems at Kawagoe and Vielsalm, in contrast to those at KHEW and ChNNF, are (1) that the actual lag times were rather longer than the expected lag times, and (2) that the flow velocity of the main sample tubes were higher and, consequently, *Re* values were slightly above the critical Reynolds number ($Re = 2300$). Further, the flow rates of these two sites were correctly measured and determined (M. Aubinet, for Vielsalm and Y. Yasuda, for Kawagoe, personal communications, 2006). In respect to the first point, some buffering effects significantly increased the response time of the two systems, although the effects did not reduce the flow rate at the point of measurement. For the second, the buffering effects might be connected with the turbulent flow rate and/or the turbulent-laminar transition in the tube flow. If so, the applicability of the theoretical transfer function may increase when the tube flow is laminar, although turbulent tube flow has been considered to be desirable for minimizing high frequency attenuation (Leuning and Judd 1996). However, this assumption is generally uncertain, because the buffering effects were not necessarily induced when tube flow was turbulent, as in the examples of NSA-OBS and Berger et al. (2001). Further, if the buffering effect of the Vielsalm system was caused by membrane filters, as suggested by Aubinet et al. (2001), it was also found in the ChNNF system. In this case, the delay time caused by a filter was larger in the Vielsalm system (0.875 s per filter) than in the ChNNF system (0.6 s per filter), in spite of the much greater flow velocity in the former.

From the discussions above, it can be considered that these buffering effects exist more or less in all other systems. The degree of the buffering effects would depend on the flow velocity and flow status, but also the many factors making up the system, such as tube bend and its angle, the arrangement of the tube, pump, filters and controllers, and their specifications. For systems in which the buffering effects were not remarkable, these effects might be converted to a slight flow decrease, so the actual lag time and expected lag time might become almost the same. In fact, the flow rate

at KHEW was adjusted by the actual lag time, although it was not contradictory to the nominal flow rate unless there was condensation. Then, on the assumption that the average flow velocity could be calculated inversely using the actual lag time minus the IRGA response time (here assuming t_{vol} plus the response time of analogue output is 0.1 s) for Vielsalm and Kawagoe, instead of the nominal flow rate, the relationships between the theoretical and empirical functions can be re-estimated (Fig. 6). In this case, the theoretical function agreed rather well with the empirical one for the Kawagoe system. This fact indicates that the unspecified buffering effects in the Kawagoe system were nearly equal to the effect of the flow rate decrease on average in the sampling tube, although actually the buffering effects might have only partially occurred, and could not be found at the flow rate measurement point. For Vielsalm, although the theoretical and empirical functions become close to each other, a significant difference remains. One of the keys to solving the remaining difference may be in the fact that the IRGA inner-chamber pressure was significantly reduced in the Vielsalm system. When a powerful pump takes in sample air through an IRGA, the inner-chamber pressure significantly reduces. Meanwhile, if the IRGA is installed after the same pump, the inner-chamber pressure increases but the difference from the ambient air pressure is not so large. If, for example, the pressure at the intake mouth is changed by a wind speed change, the effect will have a direct impact on the IRGA inner-chamber pressure in the former system. This phenomenon is probably associated with the pressure fluctuation effect, which becomes remarkable when the tube flow is turbulent, as represented by Massman (2004). However, it has not been quantified in this study, and remains to be examined in future.

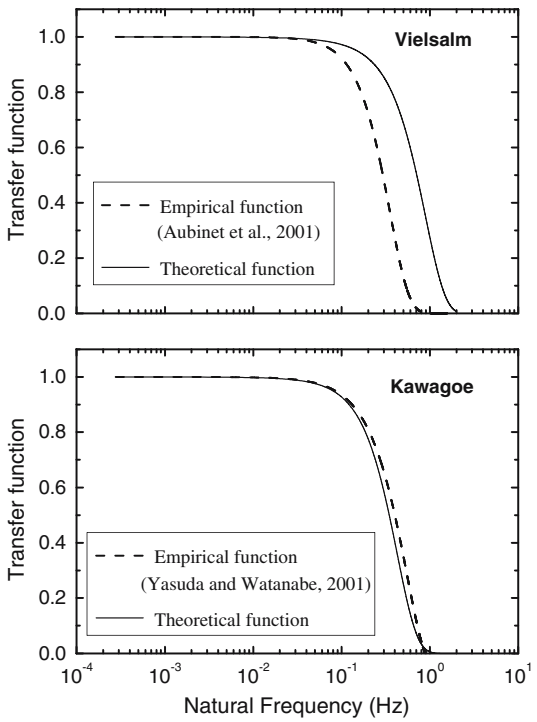

Fig. 6 Right and left panels are the same as in Fig. 5b and c, respectively, but the theoretical functions are determined by the flow rate inversely calculated from the actual response lag time of the Vielsalm and Kawagoe systems

It was found to be difficult in some measurement systems to quantify the buffering effects, and it is expected that significant disagreements between their actual frequency attenuations and the theoretical predictions will remain even if the actual lag time is used. Thus it can be concluded that an empirical correction procedure for high frequency attenuation is superior in general use compared to a theoretical one. However, it was also confirmed here that a theoretical function might be applicable in practice for some closed-path CO_2 measurement systems. The result indicates that the theoretical corrections proposed by previous studies were correctly advanced for their practical use, at least for the closed-path CO_2 flux. As described here, a theoretical function has some advantages; it enables a numerical estimate to be made of the effect of flow rate changes and variations of wind speed and direction without having to calculate the ensemble averages of scalar (co)spectra. Then, once the theoretical function has been determined as applicable, the flux computation process can be simplified and the correction process assured even when the lack of sample data to calculate the ensemble average of (co)spectra makes an empirical formulation uncertain. Therefore, there is merit in improving theories of high frequency correction by adding more factors than those used in previous studies, and so enhancing their practical application.

5 Concluding remarks

The applicability of theoretical functions to practical measurements was examined, using field measurements obtained from an Asiaflux forest site and some correction procedures described in previous studies (i.e. Goulden et al. 1997; Aubinet et al. 2001; Yasuda and Watanabe 2001; Su et al. 2004; Cook et al. 2004). The results from our field measurements suggest that for CO_2 flux measurements at the site, a theoretical function could be applied not only when the system worked normally, but also when the flow rate was reduced by condensation. This was because CO_2 concentration data might not be severely degraded by condensation in the sampling line, so long as the tube flow was not blocked or liquid water introduced into the IRGA detection chamber.

Compared to the results of previous studies, theoretical functions here did not necessarily agree with the high frequency response at each site, illustrating the limitations of the applicability of the theoretical correction for high frequency attenuation used in this study. Although the examples were limited, applicability lessened when some buffering effects within the sampling line caused an unaccountable delay. In such systems, the actual lag time, which was determined by the maximum correlation method or by the system response time measured using tracer gas blown from the intake mouth, seriously differed from the expected lag time calculated by the nominal flow rate, inner tube diameter and tube length. Using the actual lag time instead of the expected lag time made results of the theoretical function closer to the empirical one, but a significant difference between each function remained in one of the systems. The difference might be partly attributed to the effect of pressure fluctuations in the IRGA inner chamber.

However, the theoretical function was potentially applicable to the process of high frequency correction in some systems in which the actual lag time was not contrary to the expected lag time. This suggests that the various proposed theories are advancing

towards being of practical use, and indeed that there are theories already advanced enough to be applied to some systems.

It has been reported that the impact of high frequency correction on the estimate of the net ecosystem exchange is not so large, because the opposite signs of daytime and nighttime CO_2 fluxes are partially canceled out (Schmid et al. 2003). However, correction would be more important when the objective of a study is the estimates of gross primary production (GPP) and ecosystem respiration (RE) from flux measurement data. Thus information about frequency corrections will in various ways serve to increase the accuracy of GPP and RE estimations.

Acknowledgements The author is grateful to Marc Aubiinet, Faclute des Science Agronomique des Gembloux, Belgium, and Tsutomu Watanabe and Yukio Yasuda, Forestry and Forest Products Research Institute (FFPRI), for detailed information about their measurement systems and for useful suggestions. Also thanks to Koji Fukagata, University of Tokyo, Japan, for theoretical instructions about pipe flow, Yoshikazu Ohtani, FFPRI, for encouraging and supporting this study, and to the two anonymous reviewers for constructive comments on an earlier version of this paper. This study was supported by "The Long-Term CO_2 flux Observation Project (#200303)" with a grant from FFPRI.

Appendix A

Time constants of first-order functions for laminar tube flow and LI-6262

Massman (2000) successfully approximated individual correction functions as those of the first-order filters, and summarized the equivalent time constants. To add to these findings, the first-order functions for laminar tube flow, IRGA processing, and volume averaging effect of IRGA chamber are examined here. For high frequency attenuation by a turbulent tube flow, the first-order time constant is given by

$$t_{\text{tube}} = (\Lambda r L_{\text{t}})^{1/2}/(C U_{\text{t}}), \tag{A1}$$

where Λ is described in Eq. 5, C is 0.83 (Massman 2000), and t_{tube} means the equivalent time constant of the first-order filter for the tube flow attenuation. To test whether an analogy can be applied to laminar tube flow, Λ given by Eq. 6 is substituted into Eq. A1 and the time constant is obtained. This first-order function for laminar tube flow is compared to the function given by Eqs. 5 and 6, assuming a flow rate of $6\,\text{l}\,\text{min}^{-1}$ or $3\,\text{l}\,\text{min}^{-1}$, tube lengths of 5 and 50 m, and an inner diameter of 6 mm (Fig. 7), it can be seen that the first-order functions agree fairly well with Eqs. 5 and 6 for all patterns, and $C = 0.83$ is demonstrated as the best compromise for both laminar and turbulent tube flows.

The LI-6262, the most used IRGA, is considered a first-order instrument with a time constant of 0.1 s, maybe due to the response time of its analogue output. However, in reality it would be a little less than 0.1 s, as suggested by Massman (2004). Compared to $h_{3\text{B}}(\omega)$ given by Eq. 9, the most applicable constant of the first-order function, t_{IRGA}, is around 0.06 s, and the value depends on the phase factor of l_{lon}/u because of the different form of the phase function.

The volume averaging effect of the IRGA detection chamber can be aggregated as a first-order filter with the constant $t_{1\text{vol}}$ by fitting the parameter to the function $h_{\text{vol}}(\omega)$ given by Eq. 10 as the standard for comparison. For simple parameterization, $t_{1\text{vol}} = \alpha\tau_{\text{vol}}$ is assumed here, where α is a dimensionless fitted parameter. Here the $t_{1\text{vol}}$ function is considered as a form of Eq. 9, because $h_{\text{vol}}(\omega)$ does not contain the phase shift factor. An example of a comparison with $h_{\text{vol}}(\omega)$ is shown in Fig. 8.

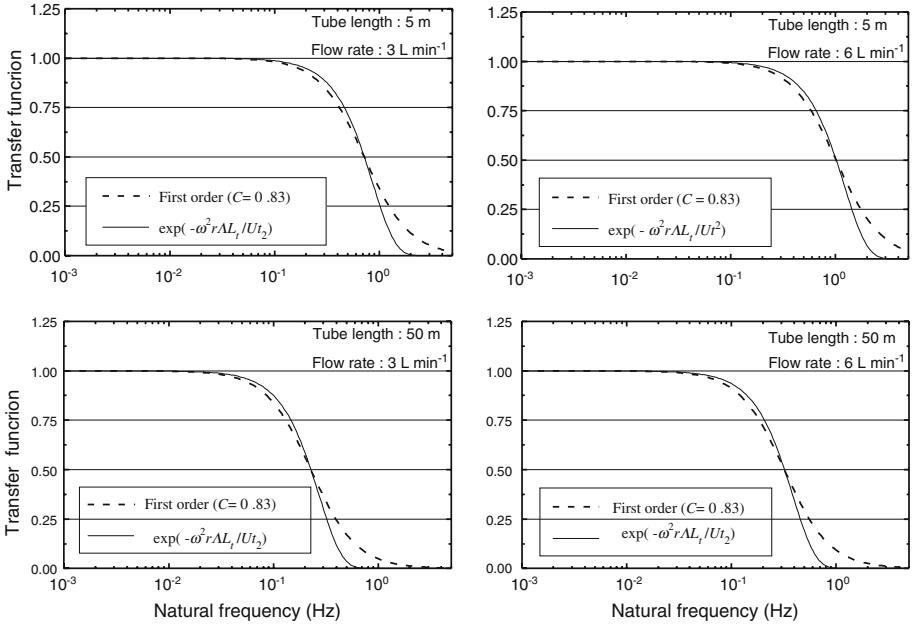

Fig. 7 Comparison of high frequency correction functions for attenuation caused by laminar tube flow. Black line: Eqs. 2 and 3 in the text. Dashed line: the approximated first-order function with the equivalent time constant calculated by substituting Eq. 3 into Eq. A1

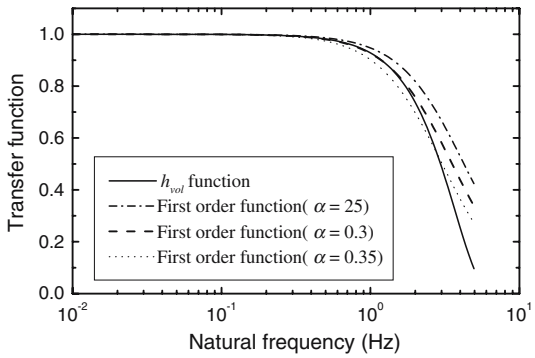

Fig. 8 An example of a comparison of the function of the IRGA volume averaging effect, $h_{\mathrm{vol}}(\omega)$ for $t_{\mathrm{vol}} = 0.15$ and the approximated first-order function with the equivalent time constant αt_{vol} for $\alpha = 0.25, 0.3$ and 0.35

Although the figure shows the single pattern of $\tau_{\mathrm{vol}} = 0.15\,\mathrm{s}$, the best-fitted α is within 0.3 ± 0.02 for possible values of τ_{vol} ($0.07\,\mathrm{s} < \tau_{\mathrm{vol}} < 0.7\,\mathrm{s}$) if a frequency range of lower than 1 Hz is mainly considered. Thus a value of 0.3 is recommended here for the parameter α regardless of the value of τ_{vol}.

Appendix B

Empirical transfer functions applied in previous studies

Note that $g(\omega)$ is a gain function and $p(\omega)$ is a phase function as in Eq. 15.

Goulden et al. (1997) adapted a recursive low-pass filter (R-C filter) for the correction of the CO_2 spectrum measured in BOREAS-NSA, comparing the virtual temperature spectrum. The filter time constant (t_r) was 0.6 s for their CO_2 flux measurement system, in which a subsample was drawn, and temperature and pressure were stabilized through the IRGA chamber. The gain and phase functions of the R-C filter, represented by Berger et al. (2001) and Massman and Lee (2002), are as follows:

$$g(\omega) = \frac{1 - A}{\sqrt{1 - 2A\cos(\omega/f_s) + A^2}}, \tag{B1}$$

$$p(\omega) = \tan^{-1}\left[\frac{A\sin(\omega/f_s)}{A\cos(\omega/f_s) - 1}\right], \tag{B2}$$

where f_s is the sampling frequency and $A = \exp(-1/f_s t_r)$. In Goulden et al. (1997), f_s was 4 Hz.

Aubinet et al. (2001) applied the following one-parameter exponential function for the high frequency correction of a closed-path CO_2 flux measured at the Vielsalm site, neglecting the phase shift factor (equivalent to $p(\omega) = 0$),

$$g(\omega) = \exp\left(-\ln(2)\frac{\omega^2}{{\omega_h}^2}\right) \tag{B3}$$

where $\omega_h = 2\pi f_h, f_h$ is the half-power frequency and is parameterized to the response of their measurement system. For the Vielsalm system, parameterization was carried out by comparisons between the cospectra of sensible heat and CO_2 fluxes. An example of $f_h = 0.3$ was represented by Aubinet et al. (2001), and this value was used for the analysis in the text.

Yasuda and Watanabe (2001) empirically parameterized the high frequency losses of their closed-path system at the Kawagoe site, on the basis of a comparison with directly measured CO_2 fluctuations using an open-path IRGA. They formulated the following exponential equations for gain and phase functions, respectively

$$g(\omega) = \sqrt{\exp\{-4.86\,(\omega/2\pi)^{1.58}\}}, \tag{B4}$$

$$p(\omega) = 1 - \exp\left\{1.09\,(\omega/2\pi)^{1.12}\right\}. \tag{B5}$$

Su et al. (2004) dealt with all the individual factors in the measurement system as one first-order filter, as in Aubinet et al. (2001), neglecting the phase shift

$$g(\omega) = \frac{1}{1 + \omega^2 {t_s}^2} \tag{B6}$$

where t_s was the parameter determined from the ratio of normalized CO_2 and sensible heat cospectra. For the analysis in the text, $t_s = 0.309$ was used, which is the average value for the summer of 2001 at the UMBS site (Su et al. 2004).

References

Aubinet M, Berbigier P, Bernhofer CH, Cescatti A, Feigenwinter C, Granier A, Grünwald TH, Havrankova K, Heinesch B, Longdoz B, Marcolla B, Montagnani L, Sedlak P (2005) Comparing CO_2 storage and advection conditions at night at different CARBOEUROFLUX sites. Boundary-Layer Meteorol 116:63–94

Aubinet M, Chermanne B, Vandenhaute M, Longdoz B, Yernaux M, Laitat E (2001) Long term carbon dioxide exchange above a mixed forest in belgian ardennes. Agric For Meteorol 108:293–315
Aubinet M, Grelle A, Ibrom A, Rannik Ü, Moncrieff J, Foken T, Kowalski AS, Martin PH, Berbigier P, Bernhofer Ch, Clement R, Elbers JA, Granier A, Grünwald T, Morgenstern K, Pilegaard K, Rebmann C, Snijders W, Valentini R, Vesala T (2000) Estimates of the annual net carbon and water exchange of forests: the EUROFLUX methodology. Adv Ecol Res 30:113–175
Baldocchi D, Falge E, Gu L, Olson R, Hollinger D, Running S, Anthoni P, Bernhofer Ch, Davis K, Evans R, Fuentes J, Goldstein A, Katul G, Law B, Lee X, Malhi Y, Meyers T, Munger W, Oechel W, PawU KT, Pilegaard K, Schmid HP, Valentini R, Verma S, Vesala T, Wilson K, Wofsy S (2001) FLUXNET: a new tool to study the temporal and spatial variability of ecosystem-scale carbon dioxide, water vapor and energy flux densities. Bull Amer Meteorol Soc 82:2415–2435
Berger BW, Davis KJ, Yi C, Bakwin PS, Zhao C-L (2001) Long-term carbon dioxide fluxes from a very tall tower in a northern forest: flux measurement methodology. J Atmos Ocean Tech 18:529–542
Brutsaert W (1992) Stability correction functions for the mean wind speed and temperature in the unstable surface layer. Geophys Res Lett 19:469–472
Cook BD, Davis KJ, Wang W, Desai A, Berger BW, Teclaw RM, Martin JG, Bolstad PV, Bakwin PS, Yi C, Heilman W (2004) Carbon exchange and venting anomalies in an upland deciduous forest in Northern Wisconsin, USA. Agric For Meteorol 126:271–295
Dyer AJ (1974) A review of flux-profile relationships. Boundary-Layer Meteorol 7:363–372
Finnigan J (1999) A comment on the paper by Lee (1998): "On micrometeorological observation of surface-air exchange over tall vegetation". Agric For Meteorol 97:55–64
Goulden ML, Daube BC, Fan S-M, Sutton DJ, Bazzaz A, Munger JW, Wofsy SC (1997) Physiological responses of a black spruce forest to weather. J Geophys Res 102(D24):28987–28996
Horst TW (1997) A simple formula for attenuation of eddy fluxes measured with first-order response scalar sensors. Boundary-Layer Meteorol 82:219–233
Horst TW (2000) On frequency response corrections for eddy covariance flux measurements. Boundary-Layer Meteorol 94:517–520
Hollinger DY, Goltz SM, Davidson EA, Lee T-J, Tu K, Valentine HT (1999) Seasonal patterns and environmental control of carbon dioxide and water vapor in an ecotonal boreal forest. Global Change Biol 5:891–902
Kaimal JC, Wyngaard JC, Haugen DA (1968) Deriving power spectra from a three-component sonic anemometer. J Appl Meteorol 7:827–834
Kristensen L, Mann J, Oncley SP, Wyngaard JC (1997) How close is close enough when measuring scalar fluxes with displaced sensors? J Atmos Ocean Tech 14:814–821
Kristensen L, Jensen NO (1979) Lateral coherence in isotropic turbulence and in the natural wind. Boundary-Layer Meteorol 17:353–373
Lee X, Black TA (1994) Relating eddy correlation sensible heat flux to horizontal sensor separation in the unstable atmospheric surface layer. J Geophys Res 99(D9):18545–18553
Lee X (1998) On micrometeorological observation of surface-air exchange over tall vegetation. Agric For Meteorol 91:29–49
Lenschow DH, Raupach MR (1991) The attenuation of fluctuations in scalar concentration through sampling tubes. J Geophys Res 96(D8):15259–15268
Leuning R, King KM (1992) Comparison of eddy-covariance measurements of CO_2 fluxes by open- and closed-path CO_2 analysers. Boundary-Layer Meteorol 59:297–311
Leuning R, Judd MJ (1996) The relative merits of open- and closed-path analysers for measurement of eddy fluxes. Global Change Biol 2:241–254
Malhi Y, Pegoraro E, Nobre AD, Pereira MGP, Grace J, Culf AD, Clement R (2002) The energy and water dynamics of a Central Amazonian rain forest. J Geophys Res 107(D20):8061, doi:10.1029/2001JD000623
Massman WJ (1991) The attenuation of concentration fluctuations in turbulent-flow through a tube. J Geophys Res 96(D8):15269–15273
Massman WJ (2000) A simple method for estimating frequency response corrections for eddy covariance systems. Agric For Meteorol 104:185–198
Massman WJ (2004) Concerning the measurement of atmospheric trace gas fluxes with open- and closed-path eddy covariance systems: the WPL terms and spectral attenuation. In: Lee X, Massman WJ, Law B (eds) Handbook of micrometeorology. Kluwer Academic Publishers, Dordrecht, pp 133–160
Massman WJ, Lee X (2002) Eddy covariance flux corrections and uncertainties in long-term studies of carbon and energy exchanges. Agric For Meteorol 113:121–144

Moncrieff JB, Massheder JM, De Bruin H, Elbers J, Friborg T, Heusinkveld B, Kabat P, Scott S, Soegaard H, Verhoef A (1997) A system to measure surface fluxes of momentum, sensible heat, water vapour and carbon dioxide. J Hydrol 188–189:589–611

Moore CJ (1986) Frequency response corrections for eddy correlation systems. Boundary-Layer Meteorol 37:17–35

Sakai RK, Fitzjarrald DR, Moore KE (2001) Importance of low-frequency contributions to eddy fluxes observed over rough surfaces. J Appl Meteorol 40:2178–2192

Schmid HP, Su H-B, Vogel CS, Curtis PS (2003) Ecosystem–atmosphere exchange of carbon dioxide over a mixed hardwood forest in Northern Lower Michigan. J Geophys Res 108(D14):4417, doi:10.1029/2002JD003011

Shimizu A, Shimizu T, Miyabuchi Y, Ogawa Y (2003) Evapotranspiration and runoff in a forested watershed, Western Japan. Hydrol Proc 17:3125–3139

Shimizu T, Suzuki M, Shimizu A (1999) Examination of a correction procedure for the flow attenuation in orthogonal sonic anemometers. Boundary-Layer Meteorol 93:227–236

Su H-B, Schmid HP, Grimmond CSB, Vogel CS, Oliphant AJ (2004) Spectral characteristics and correction of long-term eddy-covariance measurements over two mixed hardwood forests in non-flat terrain. Boundary-Layer Meteorol 110:213–253

Watanabe T, Yamanoi K, Yasuda Y (2000) Testing of the eddy covariance method for a long-term measurement of water vapour flux over a forest. Boundary-Layer Meteorol 96:473–491

Webb EK, Pearman GI, Leuning R (1980) Correction of flux measurements for density effects due to heat and water vapor transfer. Quart J Roy Meteorol Soc 106:85–100

Yasuda Y, Watanabe T (2001) Comparative measurements of CO_2 flux over a forest using closed-path and open-path CO_2 analysers. Boundary-Layer Meteorol 100:191–208